Magnetic-Field-Induced Surface Transport on Laser-Irradiated Foils

D. W. Forslund and J. U. Brackbill
Los Alamos National Laboratory, Los Alamos, New Mexico 87545

(Received 2 February 1982)

Electrons heated by absorption of laser energy are shown to generate intense magnetic fields which rapidly spread from the edge of the laser spot along the target surface. The fields convectively transport hot electrons and confine a major fraction of the deposited laser energy in the corona. Eventually, this energy is lost to fast-ion blowoff or deposited at large distances from the spot. This model qualitatively explains many experimental observations of thermal-transport inhibition and fast-ion loss.

PACS numbers: 52.25.Fi, 52.50.Jm

The generation of magnetic fields when intense laser light is absorbed in a plasma is well known.[1] It has been studied because its inhibition of electron transport would explain the inferred flux limits needed to model energy transport in laser-produced plasmas.[2] Here we report new results from fully self-consistent calculations in collisionless plasmas.[3] These show large self-generated magnetic fields in the corona which convectively transport 30% or more of the absorbed energy laterally and collimate the remainder behind the laser spot. The results appear to qualitatively explain for the first time from first principles a wide variety of experimental data on fast-ion loss and lateral transport at various laser wavelengths.

Coronal magnetic field generation by collisionless processes is modeled in the relatively simple geometry shown in Fig. 1. We consider a plasma foil 500 μm wide in y in a 600-μm-wide system with a sharp initial density gradient in x. The deposition by a 10.6-μm laser at an average absorbed intensity of 5×10^{13} W/cm^2 in a 60-μm spot is modeled by accelerating some electrons from 2.5 to about 20 keV down the density gradient in a 20° half-angle cone with maximum heating at the center. At the boundary behind the high-density material, heat is absorbed by a cool electron thermal bath. The ion to electron mass ratio is 1836. This system is numerically simulated with a two-dimensional, implicit electromagnetic simulation code, VENUS,[4] which solves Maxwell's equations and Newton's laws self-consistently for particle electrons and ions. The behavior with [(d)–(f)] and without [(a)–(c)] self-generated magnetic fields is shown in Fig. 2.

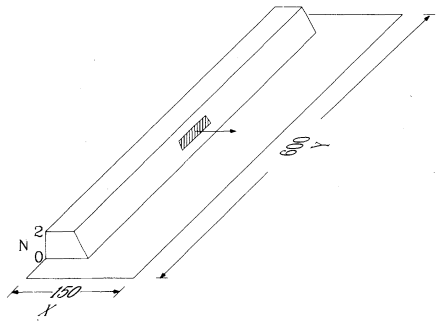

FIG. 1. Diagram showing geometry of model where the shaded box is the laser deposition region. The system is uniform in z and the maximum density is twice critical density for 10.6-μm light.

Without magnetic fields, the electrons accelerated outward return from the sheath back towards the foil. In the y-v_x phase space of Fig. 2(a), the

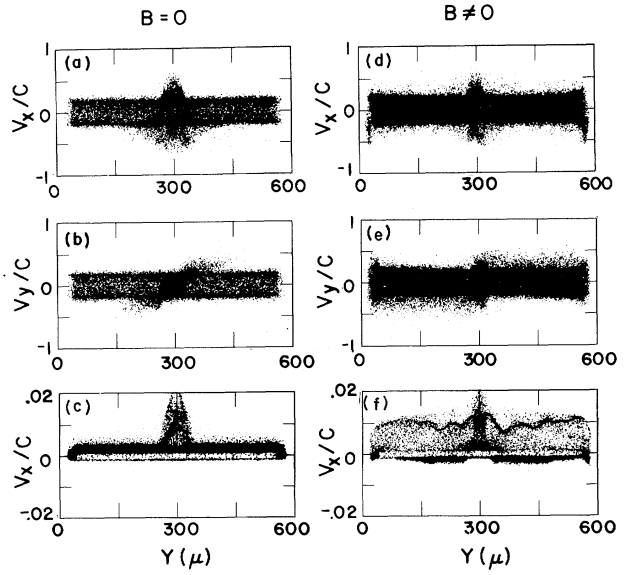

FIG. 2. Results of simulations with a 60-μm spot on a 500-μm-wide foil at 12 psec. (a)–(c) correspond to $B = 0$ and (d)–(f) correspond to $B \neq 0$. (a) and (d) are electron phase space v_x vs y for all x, (b) and (e) are electron phase space v_y vs y for all x, and (c) and (f) are ion phase space v_x vs y for all x. Only electrons with $|v| > 0.17c$ and ions with $|v| > 0.00125c$ are plotted.

increase in the spatial extent of the reflected electrons (negative v_x) arises from their small initial y velocities which are shown in Fig. 2(b). Ion acceleration [Fig. 2(c)] is localized to the laser spot where the electrons are accelerated. The energy history [Fig. 3(a)] shows that the energy flow through the back boundary is about 90% of the input, corresponding to a fast-ion loss of about 10%. This level is about twice that for a planar isothermal expansion because of scattering from the curved potential surfaces in the corona.

With magnetic fields, the returning electrons, Fig. 2(d), have the same spatial width as the original laser spot. Many electrons, as seen in Fig. 2(e), move laterally away from the laser spot. As shown in Fig. 3(b), their lateral displacement coincides with the magnetized region. Note in Fig. 2(f) that ions are accelerated not only in the laser spot but also over the entire surface of the foil. The ions respond to the magnetic field, but their gyro-orbits are large compared with the thickness of the magnetized region. The energy history [Fig. 3(a)] shows that over 30% of the absorbed energy is lost. By 12 psec, the rate of loss to the coronal fast ions is 30% of the energy absorption rate, qualitatively consistent with thick-foil experiments.[5] The magnetic field energy saturates when the lateral transport reaches the edge of the foil at about 12 psec at which time the energy is transported around the sides of the foil (Fig. 3). This saturation is consistent with the measurements of magnetic field as a function of target size.[6]

The spatially resolved electron energy flux flowing across the back boundary of the foil is shown in Fig. 4. The flux is averaged over the time interval 9–18 psec for the magnetized (solid line) and unmagnetized cases (dashed line). The results shown in Fig. 4 reproduce the experimentally observed collimation of the hot electrons to the laser spot,[7] the limb brightening of targets,[8] and the strong transport around toward the rear of disks,[9] otherwise thought to be inconsistent. The energy spectrum of electrons penetrating the foil is cooler in the presence of the self-generated magnetic field (Fig. 5) because the higher-energy electrons are trapped in the magnetic field and give up their energy to fast ions. Only lower-energy electrons are reflected in the sheath without being caught in the magnetic field. Thus, the flux penetrating the target is reduced at the expense of the more energetic electrons. The magnetic field alters the source of hot electrons reaching high-density material, but, because the field does not penetrate to high density, it should have no effect on subsequent transport at higher density. This may explain some of the apparently contradictory experimental data.[5]

An approximate expression[2] for the source of

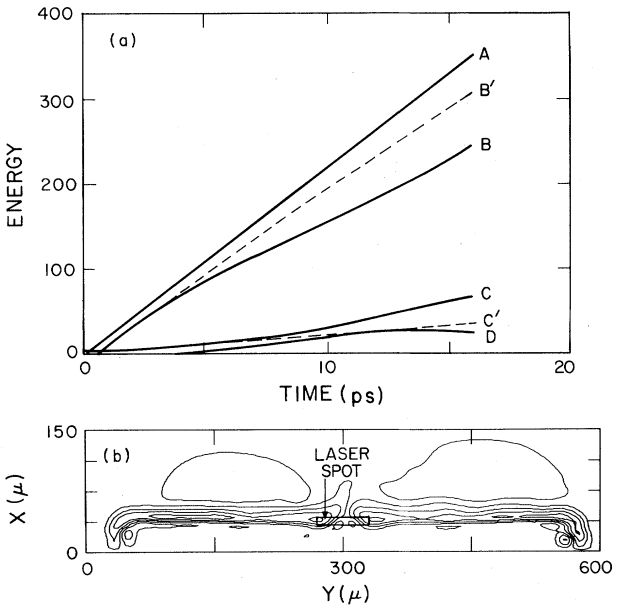

FIG. 3. The energy in various plasma components as a function of time is shown in (a) with dashed curves corresponding to $B = 0$ and solid curves for $B \neq 0$. Curve A shows the total absorbed energy; B and B', the total energy transported across the back boundary; C and C', the total ion kinetic energy; and D, the total magnetic field energy. Magnetic field contours on the foil at 12 psec are shown in (b). The peak field is ± 1.3 mG and the contour interval is 0.33 mG.

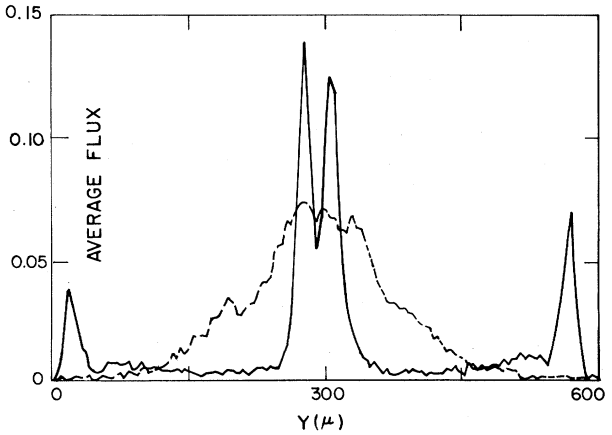

FIG. 4. Integrated energy transport across the back of a foil as a function of position on the foil. The dashed line corresponds to $B = 0$ and the solid line to $B \neq 0$.

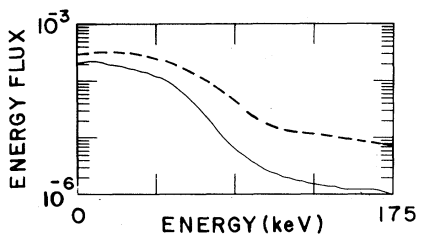

FIG. 5. Time-averaged electron spectrum of net energy transported across the entire back foil boundary. The curve is the integral of all energy transported above that energy. The dashed line is for $B = 0$, and the solid line is for $B \neq 0$.

the magnetic field in this model is given in the collisionless limit by $\vec{B} = \nabla \times \nabla \cdot \vec{\Pi}/n_e$, where $\vec{\Pi}$ is the electron pressure tensor. With an initial density gradient length L_n in x and a temperature gradient length L_T in y, the magnetic field increases at the rate $\dot{\Omega}_e = v_e^2/L_n L_T$, where v_e is the hot-electron thermal speed and Ω_e is the electron gyrofrequency. The magnetic field is generated at the edge of the laser spot where gradients are largest. Saturation occurs in the simulations because of finite magnetic pressure. Since the peak magnetic pressure is observed to be of the order of the plasma pressure, the lateral electron $\vec{E} \times \vec{B}$ drift is estimated to be $v_d/v_e \sim c/\omega_{pe} L_n$, independent of spot size, similar to a thermal magnetic wave.[10] The high coronal pressure induced by the magnetic field maintains a density gradient of order of c/ω_{pe} and thus the high lateral drift speed. The magnetic field is localized as a result of the large return current of cooler electrons drawn along the surface at higher densities. This magnetic boundary layer structure is reminiscent of the properties of a rarefaction shock.[11] It is also apparently the thermal analog of parapotential flow present in magnetically insulated diodes.[12]

From Fig. 3, absorbed laser energy trapped in the corona is proportional to the magnetic field energy. From the field generation rate and the assumption of a plasma β of order unity, the ratio of the rate of field generation to input energy flux is proportional to $c/\omega_{pe} R$, where R is the spot radius. Thus the larger the spot size or the higher the plasma density the smaller the initial magnetic field generation rate and the lower the fast-ion loss.

The speed of convective transport in the magnetic field is enhanced by the directionality of electron acceleration in resonant absorption. The magnetic field is no less important in cases where the electrons are heated isotropically[13] where more of the outward directed energy should be trapped in the corona until lost to ion motion. Modeling this process in general with an isotropic flux limit in the diffusion approximation is questionable and it should not be surprising that there have been difficulties with one-dimensional modeling of flat-target experiments. For example, this model seems to explain the asymmetry in plasma expansion between the front and back side of laser-irradiated disks[14] which cannot be accounted for by simple one-dimensional models.[15] Field generation should occur also at shorter wavelengths (which deposit energy in more collisional plasmas) provided $\Omega_c \tau > 1$, where τ is the electron-ion collision time, so that pressure effects dominate magnetic diffusion. Since the field generation depends upon sharp density gradients, a plasma with much gentler gradients, such as a gas jet,[16] may not be as susceptible to magnetic-field–modified transport.

In short, self-generated magnetic fields near the laser deposition region convectively transport electrons along the target surface causing substantial fast-ion loss from an extended region. The results appear to match qualitatively a variety of experimental data on inhibited electron transport and fast-ion loss.

This work was performed under the auspices of the U. S. Department of Energy.

[1]J. Stamper and B. H. Ripin, Phys. Rev. Lett. 34, 138 (1975).

[2]C. E. Max, W. M. Manheimer, and J. J. Thomson, Phys. Fluids 21, 128 (1978).

[3]J. M. Kindel, Bull. Am. Phys. Soc. 20, 1230 (1975); E. L. Lindman, D. W. Forslund, J. M. Kindel, K. Lee, and W. R. Shanahan, Bull. Am. Phys. Soc. 20, 1378 (1975).

[4]J. U. Brackbill and D. W. Forslund, to be published.

[5]G. Tsakiris, K. Eidmann, R. Petsch, and R. Sigel, Phys. Rev. Lett. 46, 1202 (1981).

[6]A. Raven, P. T. Rumsby, J. A. Stamper, O. Willi, R. Illingworth, and R. Thareja, Appl. Phys. Lett. 35, 526 (1979).

[7]R. Decoste, J.-C. Kieffer, and H. Pépin, Phys. Rev. Lett. 47, 35 (1981).

[8]P. A. Jaanimagi, N. A. Ebrahim, N. H. Burnett, and C. Joshi, Appl. Phys. Lett. 38, 734 (1981).

[9]N. A. Ebrahim, C. Joshi, D. M. Villeneuve, N. H. Burnett, and M. C. Richardson, Phys. Rev. Lett. 43, 1995 (1979).

[10]G. J. Pert, J. Plasma Phys. 18, 227 (1977).

[11]B. Bezzerides, D. W. Forslund, and E. L. Lindman,

Phys. Fluids 21, 2179 (1978).
[12]O. Buneman, Proc. Cambridge Philos. Soc. 50, 77 (1954).
[13]R. J. Mason, Phys. Rev. Lett. 42, 239 (1979).
[14]R. Decoste, S. E. Bodner, B. H. Ripin, E. A. McLean, S. P. Obenschain, and C. M. Armstrong, Phys. Rev. Lett. 42, 1673 (1979).
[15]S. J. Gitomer, E. A. McLean, B. H. Ripin, and F. C. Young, Los Alamos Report No. LA-UR-79-2473, 1979 (unpublished).
[16]F. Mayer, Gar. E. Busch, G. Charatis, D. K. Jarrell, R. J. Shroeder, D. C. Slater, and J. A. Tarvin, in Proceedings of the Eleventh Annual Anomalous Absorption Conference, 1981 (unpublished), paper 5-2.

Nonuniversal Critical Behavior of Micellar Solutions

Mario Corti
Centro Informazioni Studi Esperienze, 20100 Milano, Italy

and

Vittorio Degiorgio
Istituto di Fisica Applicata, Università di Pavia, 27100 Pavia, Italy

and

Martin Zulauf
European Molecular Biology Laboratory, Grenoble Outstation, 156X, F-38042 Grenoble-Cedex, France

(Received 5 April 1982)

The critical behavior of two nonionic-amphiphile solutions showing a lower consolution point is investigated by laser-light scattering. The critical exponents γ and ν take the values $\gamma=1.15$ and $\nu=0.57$ for the system H_2O-C_8Et_4, and $\gamma=0.90$ and $\nu=0.44$ for H_2O-$C_{12}Et_8$. Both sets of values are different from those previously found with the system H_2O-$C_{12}Et_6$. The description of the observed nonuniversality of critical micellar solutions may require three-dimensional models which exhibit continuously varying critical exponents.

PACS numbers: 64.60.Fr, 05.70.Jk, 82.70.Dd, 87.15.Da

There is a growing awareness of the importance of critical phenomena for the description of the thermodynamic and transport properties of micellar solutions[1,2] and microemulsions.[3] A detailed knowledge of the phase-transition mechanism in such systems, besides its intrinsic interest, is strongly relevant for the biochemical applications of nonionic amphiphiles[4] and for the chemical engineering use of microemulsions. The experimental results previously obtained with the critical binary mixture water–*n*-dodecyl hexaoxyethylene glycol monoether ($C_{12}Et_6$) have shown that the solution properties in a temperature region extending 20°C below the lower consolution point are mainly determined by critical concentration fluctuations.[1] An unexpected result reported in Ref. 1 is that the measured critical exponents ($\gamma=0.97\pm0.05$, $\nu=0.53\pm0.05$) were found to disagree with those measured in usual critical binary mixtures and predicted by the three-dimensional Ising model. In order to test the interpretation of the previous results and to gain further information on the critical behavior of micellar solutions, we have studied by light scattering two nonionic amphiphiles similar to $C_{12}Et_6$, but with different monomer lengths, namely, C_8Et_4 and $C_{12}Et_8$. Our data show that the values of the critical exponents depend on the nature of the amphiphile. Clearly this result is not compatible with the Ising model or with the equivalent predictions of Wilson renormalization-group theory.[5]

The compound C_8Et_4 was synthetized and purified by Grabo *et al.*[6] High-purity $C_{12}Et_8$ was obtained from Nikko Chemicals, Tokyo. The sample preparation procedure and the light-scattering apparatus are the same as in Ref. 1. The scattering angles used were 22° and 90°.

The phase diagram of C_8Et_4 in H_2O at atmospheric pressure is shown in Fig. 1. The curve of critical micelle concentration (cmc, the concentration above which micelles are formed; this should not be confused with the concentration c_c